Vanadium $L_{2,3}$ XANES Experiments and First Principles Multielectron Calculations: Impact of Second-Nearest Neighbouring Cations on Vanadium-Bearing Fresnoites

Thomas Höche
Fraunhofer-Institut für Werkstoffmechanik IWM
Walter-Hülse-Straße 1, D - 06120 Halle, Germany

Hidekazu Ikeno
Fukui Institute for Fundamental Chemistry
Kyoto University, Takano-Nishihiraki, Sakyo, Kyoto 606-8103, Japan

Marisa Mäder
Leibniz-Institut für Oberflächenmodifizierung e.V.
Permoserstraße 15, D - 04318 Leipzig, Germany

Grant S. Henderson
Department of Geology, University of Toronto
22 Russell Street, Toronto, M5S 3B1 Canada

Robert I.R. Blyth
Canadian Light Source, University of Saskatchewan
101 Perimeter Road, Saskatoon, S7N OX4, Canada

Brian C. Sales
Correlated Electron Materials Group, Materials Sciences and Technology Division
Oak Ridge National Laboratory, Oak Ridge, TN 37831-6056, U. S. A.

Isao Tanaka
Department of Materials Science and Engineering
Kyoto University, Yoshida, Sakyo, Kyoto 6006-8501, Japan

Key Words: X-ray absorption spectroscopy (V-$L_{2,3}$ XANES), first principles multielectron theory, fresnoites, $Ba_2VSi_2O_8$, $K_2VV_2O_8$, $Rb_2VV_2O_8$

This is a preprint, the final version is subject to change, of the American Mineralogist (MSA)
Cite as Authors (Year) Title. American Mineralogist, in press.
(DOI will not work until issue is live.) DOI: http://dx.doi.org/10.2138/am.2013.4335

ABSTRACT

Transition-metal $L_{2,3}$ XANES spectra are widely used to determine coordination and valence of the target ion. For decades, experimental fingerprinting, i.e., the comparison with spectra obtained from known reference compounds was the way to interpret spectral features. This approach was based on the common understanding that only anions in the first coordination sphere would determine the near-edge structure, and crystalline references were selected accordingly. Using *ab initio* charge-transfer multiplet calculations, we demonstrate that there is also a significant impact on spectral features from the second-nearest neighbour cations. This finding is exemplified for three fresnoite-type vanadates, namely $Ba_2VSi_2O_8$ (BVS), $K_2VV_2O_8$ (KVV), and $Rb_2VV_2O_8$ (RVV). The theoretical treatment provides evidence that for the three compounds studied it is not variable bond lengths or bond angles between vanadium and oxygen that make the V-$L_{2,3}$ XANES spectra different, but the interaction of the target vanadium ions with its neighbouring cations (Si for BVS, V for KVV & RVV) which dominates. Therefore, we conclude that simple fingerprinting can result in misleading interpretations when interactions with second-nearest neighbouring cations are not taken into account. *Ab initio* charge-transfer multiplet calculations of spectral shapes (theoretical fingerprinting) should be employed instead to get a deeper understanding of structure-spectra relationships, or the choice of reference spectra should take into account second-nearest neighbours. Our findings are similarly important for the interpretation of electron energy-loss near-edge (ELNES) spectra.

INTRODUCTION

The spectroscopy of unoccupied states, either excited by X-rays (X-ray absorption near-edge structure, XANES) or electrons (electron energy loss near-edge structure, ELNES) has been

gaining increasing interest due to its sensitivity towards subtle changes in the electronic structure accessible at a spectral resolution below 100 meV, or more precisely 10^{-4} times the excitation energy (Regier et al., 2007).

It has been known for many years that departures in coordination around the probed transition-metal ion (see e.g. (Brydson et al., 1989)) do result in changes to the spectral shape of transition-metal $L_{2,3}$ edges. This is because the energetic position of unoccupied 3d states is sensitively influenced by the crystal-field splitting essentially caused by the anions in the first coordination sphere around the probed cation (Höche et al., 2004). Another source of spectral differences is the valence state. For transition metals, it is found that lowering the valence causes a chemical shift towards lower photon energies or electron energy losses, respectively (Leapman et al., 1982). This chemical shift is due to more effective screening of the core potential for reduced species. In parallel, upon decreasing the valence of a given element, the number of unoccupied states is decreased as well. For example, chemical shifts of the Ti $L_{2,3}$ edges towards lower energy losses have been observed by Leapman (Leapman et al., 1982), while $La_{1-x}Sr_xTiO_3$ was studied by Abbate *et al.* (Abbate et al., 1991) using Ti-$L_{2,3}$ XANES to demonstrate the influence of altering Ti valence while keeping the Ti coordination unchanged (via the substitution of strontium by lanthanum). Höche *et al.* (Höche et al., 2003b) also proved this effect using ELNES spectroscopy of barium oxo titanates (III/IV) $Ba_xTi_{2x}^{3+}Ti_{8-2x}^{4+}O_{16}$. Eventually, Coulomb and exchange interactions(Zaanen et al., 1985) have to be taken into account for understanding departures from the ideal L_3/L_2 intensity ratio for 3d transition metals (Thole and Laan, 1988).

While the experimental assessment of transition-metal $L_{2,3}$ edges has been brought to a very high level of sophistication in terms of spectral, as well as, spatial resolution, the simulation of transition-metal *L*-edges has only recently reached a state where interpretation and

This is a preprint, the final version is subject to change, of the American Mineralogist (MSA)
Cite as Authors (Year) Title. American Mineralogist, in press.
(DOI will not work until issue is live.) DOI: http://dx.doi.org/10.2138/am.2013.4335

predictions are feasible (Ikeno et al., 2009; Ikeno et al., 2006; Ikeno et al., 2005; Kumagai et al., 2008).

The apparent advantages of *ab initio* charge-transfer multiplet (CTM) calculations were demonstrated for 3d metals by consideration of electronic configurations in the configuration interactions. With this approach, not just qualitative but *quantitative* reproduction of ELNES or XANES spectra is possible. While in earlier studies (Ikeno et al., 2011), compounds hosting transition metals in single valence and coordination states have been dealt with, here, we go one step further by considering three fresnoite-type vanadates, namely $Ba_2VSi_2O_8$, $K_2VV_2O_8$, and $Rb_2VV_2O_8$, the last two of which host vanadium in two valance states and coordinations.

The structural peculiarity of fresnoite compounds lies in the fact that this framework structure hosts pentahedrally coordinated transition metals. In the case of $Ba_2VSi_2O_8$ (BVS) (Höche et al., 2003a), tetravalent vanadium occurs exclusively in a square pyramid consisting of four basal-plane oxygen ions with identical distances to the central vanadium ion and one apical oxygen ion connected via a short double bond forming a vanadyl group (cf. Table 1).

Apart from the single-valance, single-coordination V-bearing compound BVS, we have also studied two other fresnoite framework structures featuring one tetravalent vanadium position in pentahedral coordination *plus* one pentavalent vanadium position in tetrahedral coordination. Substitution of the Si positions in BVS by V^{5+} requires charge compensation that can be accomplished by a parallel substitution of the alkaline earth metal Ba^{2+} by an alkali metal, e.g., K^+ or Rb^+. The V-$L_{2,3}$ ionization edges of $K_2VV_2O_8$ (KVV)(Galy and Carpy, 1975) and $Rb_2VV_2O_8$ (RVV)(Ha-Eierdanz and Müller, 1992; Withers et al., 2004) are

This is a preprint, the final version is subject to change, of the American Mineralogist (MSA)
Cite as Authors (Year) Title. American Mineralogist, in press.
(DOI will not work until issue is live.) DOI: http://dx.doi.org/10.2138/am.2013.4335

therefore characterised by a rather complex, weighted superposition of V(d) states stemming from the $V^{4+}O_5$ pyramid with electronic states related to two identical $V^{5+}O_4$ tetrahedra.

Using soft X-ray XANES data acquired at the SGM beamline of the Canadian Light Source, the extent to which *ab initio* CTM calculations at the V-$L_{2,3}$ ionization edge of the two oxo vanadates (IV/V) KVV and RVV can reproduce experimental data was studied.

EXPERIMENTAL METHODS

About 100 grams of V_2O_5 and 76 grams of K_2CO_3 (or Rb_2CO_3) are loaded into a 250 ml Pt crucible, slowly heated in air to 700 °C and held for 2 h. The powder is added in two stages because of substantial foaming. The molten KVO_3 ($RbVO_3$) flux is then cooled to room temperature and the Pt crucible and solidified KVO_3 ($RbVO_3$) loaded into a fused silica ampoule that is necked down at the top. Using a long funnel, 9 g of VO_2 is added to the Pt crucible and the entire ampoule is evacuated and sealed. The sealed ampoule is loaded into a furnace, heated to 850 °C for 6 h, cooled to 700 °C over 1 h and then cooled to about 400 °C at 1 °C/h, followed by furnace cooling to room temperature. The KVO_3 ($RbVO_3$) flux is then removed with a combination of warm water and ultrasonic vibration. The resulting $K_2V_3O_8$ or $Rb_2V_3O_3$ crystals are black rectangular plates with dimensions as large as 5 x 5 x 1 mm^3.

As described elsewhere (Höche et al., 2003a), high-purity $Ba_2VSi_2O_8$ was prepared via a sol-gel route. The light blue coloured powder obtained this way was ground, pressed into pellets and sintered under a dry argon atmosphere at 750 °C for 16 h using a heating rate of 3 K/min. The black pellets obtained were crushed, ground and pressed again. Sintering was completed at 1,150 °C for 16 h under a dry argon atmosphere and resulted in grey-green pellets of $Ba_2VSi_2O_8$ as confirmed by X-ray powder diffractometry.

This is a preprint, the final version is subject to change, of the American Mineralogist (MSA)
Cite as Authors (Year) Title. American Mineralogist, in press.
(DOI will not work until issue is live.) DOI: http://dx.doi.org/10.2138/am.2013.4335

V-$L_{2,3}$ edge XANES data of $K_2VV_2O_8$ and $Rb_2VV_2O_8$ single crystals as well as a $Ba_2VSi_2O_8$ polycrystal were recorded in the energy range between 510 and 529 eV at the spherical-grating monochromator (SGM) beamline of the Canadian Light Source using a step width of 50 meV (in the hi-res mode: 20 meV) and an exit slit of 20 microns. Since the probing depth of the total electron yield (TEY) data is only on the order of a few nanometers, and hence superficial effects may be emphasized, fluorescence-yield (FLY) data were used throughout this study. For calibration, a CO spectrum was recorded and the photon energy scale was calibrated using the fifth vibrational state, known to have a value of 534.21 eV (Puttner et al., 1999). The CO spectrum also indicates the resolution - it was taken with the same settings as the other data. As its vibrational structure is well-resolved, the resolution is around 80 meV.

THEORETICAL METHODS

A number of theoretical methods have been used to obtain theoretical XANES/ELNES from first principles, which is described in a series of review papers (Mizoguchi et al., 2010; Tanaka and Mizoguchi, 2009; Tanaka et al., 2005). A supercell core-hole method on the basis of density functional theory (DFT) is the most popular method. However, it cannot be used for $L_{2,3}$ XANES/ELNES of 3d-transition metal (TM) elements, since widely spread multiplet structures due to the localized 3d electrons dominate the spectra. The presence of a 2p-core hole introduces further complexity into the spectra. Recently, a first principles method has been developed to deal with the electronic correlations among 3d electrons and a 2p core-hole (Ikeno et al., 2009; Ikeno et al., 2006; Ikeno et al., 2005; Kumagai et al., 2008).

This can be made by taking all Slater determinants produced from relativistic molecular spinors. In the quantum chemistry terminology, this is the configuration interaction (CI)

calculation using molecular spinors via DFT. In addition to the TM-3d atomic spinors, ligand atomic spinors sometimes play essential roles in the TM-$L_{2,3}$ XANES/ELNES. An additional atomic configuration, that is, $3d^n + 3d^{n+1}\underline{L}$ for the initial state and $2p^5 3d^{n+1} + 2p^5 3d^{n+2}\underline{L}$ for the final states, where $\underline{L}$ denotes a hole on ligand spinors, should be taken into account. The multiplet structures in such cases are called charge-transfer multiplet (CTM). In the present study, we made a set of CTM calculations by the DFT+CI approach.

Relativistic molecular spinor calculations were carried out by solving Dirac equations employing the local density approximation (LDA). Four-component relativistic molecular spinors were expressed as linear combinations of atomic spinors. The numerically generated four component relativistic atomic spinors (1s - 4p for V and 1s - 2p for O) were used as basis functions for molecular spinors. Cluster models composed of one V ion and the coordinating oxygen ions were used for the calculation. The total number of electrons in the cluster was counted on the basis of the formal charges of the constituents. Therefore, the clusters were VO_5^{6-} for V^{4+}, and VO_4^{3-} for V^{5+}. Charge-transferred configurations having a single ligand hole were considered but configurations with two or more ligand holes were not considered in the present study.

The positions of the atoms in the crystalline compounds were obtained from the experimental crystal structures. To take account of the effective Madelung potential, an array of point charges was placed at the external atomic sites of clusters using the method proposed by Evjen (Evjen, 1932).

The number of Slater determinants for VO_5^{6-} is 23,230, namely ${}_{10}C_1 + {}_{10}C_1 \times {}_{30}C_{29} = 1{,}360$ for initial states and ${}_6C_5 \times {}_{10}C_2 + {}_6C_5 \times {}_{10}C_3 \times {}_{30}C_{29} = 21{,}870$ for final states. The number for VO_4^{3-} is 6,781, namely ${}_{10}C_0 + {}_{10}C_1 \times {}_{24}C_{23} = 341$ for initial states and ${}_6C_5 \times {}_{10}C_1 + {}_6C_5 \times {}_{10}C_2 \times {}_{24}C_{23} =$

This is a preprint, the final version is subject to change, of the American Mineralogist (MSA)
Cite as Authors (Year) Title. American Mineralogist, in press.
(DOI will not work until issue is live.) DOI: http://dx.doi.org/10.2138/am.2013.4335

6,540 for final states. The number of Slater determinants corresponds to the number of many electron eigenvalues or multiplets.

Theoretical XANES/ELNES was obtained as the oscillator strength of the electric dipole transition using the many-electron wave functions for the initial and final states. The photoabsorption cross section (PACS) was obtained by broadening the oscillator strengths using Lorentz functions and by multiplying by the constant $2\pi^2\hbar^2\alpha/m$, where α is the fine-structure constant (=1/137.036). The other terms are of usual meaning. The full width at half-maximum (FWHM) of the Lorentz function was set to 0.4 eV over the whole energy region. The quadrupole and higher order transitions were ignored.

This CI method is known to systematically overestimate the absolute transition energy (Ogasawara et al., 2001). This can be ascribed to the truncation of the Slater determinants. In other words, this is due to disregarding the minor contribution of the electronic correlations. In the present study, the transition energy was corrected by taking the energy difference between molecular spinors for the Slater's transition state as a reference. More details on the method are described in (Ikeno et al., 2011).

RESULTS AND DISCUSSION

Single crystals of $Ba_2VSi_2O_8$ (Höche et al., 2003a), $Rb_2V^{4+}V_2^{5+}O_8$ (Withers et al., 2004), and $K_2V^{4+}V_2^{5+}O_8$ (Galy and Carpy, 1975) were grown as described in the experimental section and confirmed to be single-phase by standard X-ray diffraction techniques. All three compounds crystallize in the fresnoite framework structure, named after the mineral fresnoite, $Ba_2TiSi_2O_8$ (Alfors et al., 1965) (space group *P4bm*) (Moore and Louisnathan, 1967). In the general formula $A_2PT_2O_8$ (see Fig. 1), "T" denotes a tetrahedrally coordinated ion (Si^{4+}, Ge^{4+},

This is a preprint, the final version is subject to change, of the American Mineralogist (MSA)
Cite as Authors (Year) Title. American Mineralogist, in press.
(DOI will not work until issue is live.) DOI: http://dx.doi.org/10.2138/am.2013.4335

or V^{5+}), "A" an alkali ion (such as K, or Rb) or an alkaline-earth ion (Ba or Sr) and "P" is Ti^{4+} or V^{4+} in pentahedral coordination. The fresnoite crystal structure is comprised of corner-connected "T"$_2O_7$, and "P"O_5 square pyramids arranged in sheets interspersed with layers of "A" ions.

Fresnoite structures are very susceptible to the formation of incommensurate structural modulations (Höche et al., 1999; Withers et al., 2002) but such modulations are neither observed for $K_2VV_2O_8$, $Rb_2VV_2O_8$, nor $Ba_2VSi_2O_8$ at room temperature. In order to interpret departures in their respective XANES spectra, their crystal structures in terms of bond length and bond angles will be discussed in a bit more detail. While the bond lengths within the VO_5 pyramid of the three compounds vary by up to 10 % (for the vanadyl bonding with the apical oxygen) and by up to 5 % for the bonding towards the basal oxygen (Tab. 1), the shape of the VO_5 group itself is relatively unchanged (Tab. 2). Comparing bond lengths in the V_2O_7 groups of $K_2VV_2O_8$ and $Rb_2VV_2O_8$ (Tab. 2 and Fig. 2), it is found that bond lengths in $K_2VV_2O_8$ are generally circa 5 % longer than corresponding distances in $Rb_2VV_2O_8$. Bond angles of the V_2O_7 groups, however, clearly differ by less than 1 % (Tab. 3). This means that structural discrepancies between $K_2VV_2O_8$ and $Rb_2VV_2O_8$ mainly concern bond lengths rather than bond angles. Hence, these two samples are very well suited to experimentally address the influence of bond length on the electronic structure of unoccupied states.

Experimental V-$L_{2,3}$ XANES of KVV/RVV are compared to that of BVS in Fig. 3. Peaks are denoted by letters for ease of discussion and as guides for the eye. Roughly speaking, peaks “A” to “E” and “a” to “e” can be attributed to the L_3 edge. The rest of the peaks are attributable to L_2 edges. Although the valency and coordination number of V are clearly different between KVV/RVV and BVS, there is a rough similarity in V-$L_{2,3}$ XANES among these three compounds. This implies that analysis of valency and coordination number (C.N.)

This is a preprint, the final version is subject to change, of the American Mineralogist (MSA)
Cite as Authors (Year) Title. American Mineralogist, in press.
(DOI will not work until issue is live.) DOI: http://dx.doi.org/10.2138/am.2013.4335

by the experimental V-$L_{2,3}$ XANES alone (e.g., the often applied fingerprinting) is difficult. Theoretical V-$L_{2,3}$ XANES spectra of the three compounds are depicted in Fig. 4. Since there are two kinds of V sites i.e., V^{4+} (C.N.=5) and V^{5+} (C.N.=4) in KVV/RVV, we made *ab initio* CTM calculations separately for each site. The weighted sum of two spectra by 1:2 corresponds to the theoretical spectra of RVV/KVV. On the other hand, the theoretical spectrum for BVS was obtained only for a single V^{4+} (C.N.=5) site.

The agreement between experimental and theoretical spectra for the three compounds is quite good. Small discrepancies in relative peak positions, intensities, and widths may be attributable to small insufficiencies in the models for the calculations. The largest problem may be the neglect of the interactions among V-3d electrons on different sites. Since the calculations were made with clusters composed of only one V ion coordinated by four or five oxide ions, off-site d-d exchange and correlation interactions were ignored. Only the electrostatic part (Madelung potential) of the solid state effects due to embedding the cluster into the crystalline environment were taken into account. This is one of the reasons why the theoretical spectra are generally sharper than the experimental spectra. Nevertheless the quality of the theoretical spectra is sufficient to discuss the details of the experimental spectra.

The chemical shift between the peak-maxima of V^{4+} (C.N.=5) and V^{5+} (C.N.=4) in KVV/RVV is only 0.5 eV (Fig. 4). This is the reason why the energy of the peak maxima cannot be clearly discriminated between RVV/KVV and BVS by experiments (Fig. 3). Moreover, the general shape of the RVV/KVV/BVS spectra, all with low-energy shoulders being present, i.e., “C” and “c” in the L_3 edge and “F” and “f” in the L_2 edge, looks similar at first glance. In order to explain this behavior, calculations prove very helpful.

Figure 5 separately compares components of V^{4+} (C.N.=5) and V^{5+} (C.N.=4) in the three compounds. The components of V^{5+} (C.N.=4) in KVV and RVV are almost identical. As described earlier, the structural discrepancies in VO_4 tetrahedra between KVV and RVV mainly concern bond lengths rather than bond angles. Although the bond lengths are different by circa 5%, the spectra are not changed significantly.

The components of V^{4+} (C.N.=5) in KVV and RVV are almost identical, too. This may be the same story as that of V^{5+} (C.N.=4): The spectrum is not sensitive to the bond-lengths. On the other hand, the V^{4+} (C.N.=5) components in KVV and RVV are clearly different from that of BVS (Fig. 5, bottom). The lower energy shoulder of the L_3 peak is sharper in BVS. It is the same for the L_2 peak. This is interesting since BVS has the same crystalline structure as that of KVV/RVV and the shapes of the VO_5 pyramids in KVV/RVV and BVS are similar except for the difference in the bond length. This can be ascribed to the valency difference of cations located at the tetrahedral sites: In the case of BVS, Si^{4+} is located in the tetrahedral site, while this site is occupied by V^{5+} in the case of KVV/RVV. This results in a difference of the spatial distribution of the Madelung potential around the V^{4+} in the VO_5 pyramid as the second-nearest neighbors of V^{4+} are V^{5+} rather than Si^{4+}.

An analogous result was reported for Co-$L_{2,3}$ XANES of trivalent cobalt oxides (Kumagai et al., 2008). The spectra for $LaCoO_3$ at low temperature and for $LiCoO_2$, both of which have low-spin Co^{3+} ions in similar local environments exhibit clear differences in peak shape. The reason was well explained by the difference in the crystal structure as modeled by the spatial distribution of the Madelung potential.

Although both V^{4+} (C.N.=5) and V^{5+} (C.N.=4) components in KVV and RVV are almost identical in shape, there are subtle differences in the peak positions of the V^{5+} (CN=4)

components. This can be ascribed to the difference in the magnitude of the Madelung potential caused by the difference in the bond lengths. The tiny difference makes the spectral shape of KVV and RVV slightly different after summing up the V^{4+} (C.N.=5) and V^{5+} (C.N.=4) components. Both the centers of the L_3 and L_2 peaks move slightly to lower energy in RVV as compared to KVV. The direction of the energy shift agrees with the observed trend in the experimental spectra (Fig. 3).

Finally, limits of fingerprinting of XANES by experimental data should be pointed out. Experimental fingerprinting techniques try to correlate spectral features with the corresponding local structures such as the $V^{5+}O_4$ tetrahedron and $V^{4+}O_5$ pyramid. Since BVS has only a single V site, spectral features such as the presence of the shoulder peaks C, D and F in BVS might be mistakenly used as the fingerprints of V^{4+} (C.N.=5). However, as can be clearly seen in Fig. 4, similar peaks such as C and F can be seen even in the V^{5+} (C.N.=4) component of KVV/RVV. Moreover, peak C is not clearly seen in the V^{4+} (C.N.=5) component of KVV/RVV. The experimental fingerprinting technique may therefore lead to an incorrect interpretation. Reliable theoretical calculations are therefore essential for correct assignments.

Our results prove the necessity to employ sophisticated theoretical modelling of the transition-metal *L* edges in order to enable interpretation of the latter beyond the (at least for high spectral resolution) questionable method of fingerprinting.

ACKNOWLEDGEMENTS

The assistance of H. Schirmer and R. Keding, by that time at Otto-Schott-Institute for Glass Chemistry, University of Jena, Germany, in the preparation of $Ba_2VSi_2O_8$ is gratefully acknowledged. Research at Oak Ridge (BCS) was suported by the Materials Sciences and

320 Engineering Division, Office of Science, U. S. Department of Energy. GSH acknowledges
321 support from NSERC via a discovery grant. The Canadian Light Source is supported by
322 NSERC, NRC, CIHR and the University of Saskatchewan.

REFERENCES CITED

Abbate, M., Groot, F.M.F.d., Fuggle, J.C., Fujimori, A., Tokura, Y., Fujishima, Y., Strebel, O., Domke, M., Kaindl, G., Elp, J.v., Thole, B.T., Sawatzky, G.A., Sacchi, M., and Tsuda, N. (1991) Soft-x-ray-absorption studies of the location of extra charges induced by substitution in controlled-valence materials. Phys. Rev. B, 44(11), 5419−5422.

Alfors, J.T., Stinton, M.C., Matthews, R.A., and Pabst, A. (1965) Seven new Barium Minerals from Eastern Fresno county, California. Am. Mineralog., 50, 314-340.

Brydson, R., Sauer, H., Engel, W., Thomas, J.M., Zeitler, E., Kosugi, N., and Kuroda, H. (1989) Electron energy loss and x-ray absorption spectroscopy of rutile and anatase: a test of structural sensitivity. J. Phys. Cond. Matter, 1, 797-812.

Evjen, H.M. (1932) On the Stability of Certain Heteropolar Crystals. Phys. Rev., 39, 675.

Galy, J., and Carpy, A. (1975) Crystal-Structure of $K_2V_3O_8$ or $K_2(VO)[V_2O_7]$. Acta Cryst. B, 31, 1794-1795.

Ha-Eierdanz, M.L., and Müller, U. (1992) A New Access to Alkali Vanadates(IV,V) Crystal-Structure of $Rb_2V_3O_8$. Z. Anorg. Allg. Chemie, 613(7), 63-66.

Höche, T., Esmaeilzadeh, S., Withers, R.L., and Schirmer, H. (2003a) Structural studies on the Fresnoite type compound $Ba_2VSi_2O_8$. Z. Kristallogr., 218(12), 788-794.

Höche, T., Olhe, P., Keding, R., Rüssel, C., van Aken, P.A., Schneider, R., Kleebe, H.-J., Wang, X., Jacobson, A.J., and Stemmer, S. (2003b) Synthesis and Characterisation of Mixed-Valence Barium Titanates. Phil. Mag., 83(2), 165-178.

Höche, T., Rüssel, C., and Neumann, W. (1999) Incommensurate modulations in $Ba_2TiSi_2O_8$, $Sr_2TiSi_2O_8$, and $Ba_2TiGe_2O_8$. Solid State Commun., 110(12), 651-656.

Höche, T., van Aken, P.A., Grodzicki, M., Heyroth, F., Keding, R., and Uecker, R. (2004) Electron Energy Core-Loss Spectra of Incommensurately Modulated Crystalline and Glassy $Ba_2TiGe_2O_8$. Phil. Mag., 84(29), 3117-3132.

Ikeno, H., de Groot, F.M.F., Stavitski, E., and Tanaka, I. (2009) Multiplet calculations of $L_{2,3}$ x-ray absorption near-edge structures for 3d transition-metal compounds. J. Phys.: Condens. Matter, 21, 104208 (17 pp).

Ikeno, H., Mizoguchi, T., Koyama, Y., Kumagai, Y., and Tanaka, I. (2006) First-principles multi-electron calculations for L_2,L_3 ELNES/XANES of 3d transition metal monoxides. Ultramicroscopy, 106(11-12), 970-975.

Ikeno, H., Mizoguchi, T., and Tanaka, I. (2011) Ab initio charge transfer multiplet calculations on the $L_{2,3}$ XANES and ELNES of 3d transition metal oxides. Phys. Rev. B, 83, 155107.

Ikeno, H., Tanaka, I., Koyama, Y., Mizoguchi, T., and Ogasawara, K. (2005) First-principles multielectron calculations of Ni L-2,L-3 NEXAFS and ELNES for LiNiO2 and related compounds. Physical Review B, 72(7).

Kumagai, Y., Ikeno, H., Oba, F., Matsunaga, K., and Tanaka, I. (2008) Effects of crystal structure on Co-$L_{2,3}$ x-ray absorption near-edge structure and electron-energy-loss near-edge structure of trivalent cobalt oxides. Phys. Rev. B, 77(15) 155124.

Leapman, R.D., Grunes, L.A., and Fejes, P.L. (1982) Study of the L_{23} Edges in the 3d Transition Metals and their Oxides by Electron-ENergy-Loss Spectroscopy with Comparisons to Theory. Phys. Rev. B, 26(2), 614-635.

Mizoguchi, T., Olovsson, W., Ikeno, H., and Tanaka, I. (2010) Theoretical ELNES using one-particle and multi-particle calculations. Micron, 41, 695-709.

Moore, P.B., and Louisnathan, S.J. (1967) Fresnoite: Unusual Titanium Coordination. Science, 156, 1361-1362.

Ogasawara, K., Iwata, T., Koyama, Y., Ishii, T., Tanaka, I., and Adachi, H. (2001) Relativistic Cluster Calculation of Ligand-FieldMultiplet Effects on Cation $L_{2,3}$ X-Ray Absorption Edges of $SrTiO_3$, NiO, and CaF_2. Phys. Rev. B, 64, 115413.

Puttner, R., Dominguez, I., Morgan, T.J., Cisneros, C., Fink, R.F., Rotenberg, E., Warwick, T., Domke, M., Kaindl, G., and Schlachter, A.S. (1999) Vibrationally resolved O 1s core-excitation spectra of CO and NO. Phys. Rev. A, 59(5), 3415-3423.

Regier, T., Krochak, J., Sham, T.K., Hu, Y.F., Thompson, J., and Blyth, R.I.R. (2007) Performance and capabilities of the Canadian Dragon: The SGM beamline at the Canadian Light Source. Nucl. Instru. Meth. A, 582(1), 93-95.

Tanaka, I., and Mizoguchi, T. (2009) First-principles calculations of x-ray absorption near edge structure and energy loss near edge structure: present and future. J. Phys: Condens. Matter, 21, 104201.

Tanaka, I., Mizoguchi, T., and Yamamoto, T. (2005) XANES and ELNES in ceramic science. J. Am. Ceram. Soc., 88, 2013-2029.

Thole, B.T., and Laan, G.v.d. (1988) Branching ratio in x-ray absorption-spectroscopy. Phys. Rev. B(38), 3158-3171.

Withers, R.L., Höche, T., Liu, Y., Esmaeilzadeh, S., Keding, R., and Sales, B. (2004) A combined temperature-dependent electron and single-crystal X-ray diffraction study of the fresnoite compound $Rb_2V^{4+}V_2^{5+}O_8$. J. Solid State Chem., 177(10), 3316-3323.

Withers, R.L., Tabira, Y., Liu, Y., and Höche, T. (2002) A TEM and RUM study of the inherent displacive flexibility of the fresnoite framework structure type. Phys. Chem. Minerals, 29(9), 624-632.

Zaanen, J., Sawatzky, G.A., Fink, J., Speier, W., and Fuggle, J.C. (1985) $L_{2,3}$ Absorption Spectra of the Lighter 3d Transition Metals. Phys. Rev. B, 32(8), 4905-4913.

This is a preprint, the final version is subject to change, of the American Mineralogist (MSA)
Cite as Authors (Year) Title. American Mineralogist, in press.
(DOI will not work until issue is live.) DOI: http://dx.doi.org/10.2138/am.2013.4335

400
401

FIGURE CAPTIONS

402 Fig. 1 Graphical representation of the fresnoite framework structure. The large cations "A"
403 (Ba in BVS, K und KVV, or Rb in RVV) are interconnecting sheets of edge-
404 connected TO_4 (Si ind BVS, V^{5+} in KVV and RVV) and PO_5 (V in BVS, V^{4+} in
405 KVV and RVV) polyhedra. There are four non-equivalent oxygen positions labeled
406 O1, O2, O3, and O4.
407
408 Fig. 2 Nomenclature of vanadium and oxygen positions found in KVV and RVV.
409 While V-1 is tetravalent and fivefold coordinated, V-2 and V-3 are pentavalent and
410 fourfold coordinated.
411
412 Fig. 3 Experimental V-$L_{2,3}$ XANES spectra of BVS (upper section) and KVV and RVV
413 (lower section). Labels given to spectral features are referenced in the text.
414
415 Fig. 4 Theoretical V-$L_{2,3}$ XANES spectra of BVS (upper section) and KVV (middle
416 section) and RVV (lower section). For KVV and RVV, individual contributions of
417 V4+ and V5+ are shown separately. Instead of the experimentally measured
418 intensity, photo-absorption cross sections (PACS) are plotted versus energy.
419
420 Fig. 5 Juxtaposition of V^{4+} (upper panel) and V^{5+} (lower panel) contributions to the
421 theoretical V-$L_{2,3}$ XANES in the three compounds BVS, KVV, and RVV.
422
423
424
425

426
427
428 **Table 1** Bond lengths around vanadium atoms in $K_2VV_2O_8$, $Rb_2VV_2O_8$, and $Ba_2VSi_2O_8$
429 (cf. Fig. 2).
430

Atom 1	Atom 2	Bond length [Å]		
		$K_2VV_2O_8$	$Rb_2VV_2O_8$	$Ba_2VSi_2O_8$
V-1	O-11	1.607(5)	1.522(8)	1.663(16)
V-1	O-7	1.955(2)	1.865(4)	1.967(6)
V-1	O-8	1.955(2)	1.865(4)	1.967(6)
V-1	O-9	1.955(2)	1.865(4)	1.967(6)
V-1	O-10	1.955(2)	1.865(4)	1.967(6)
V-2	O-4	1.809(1)	1.717(2)	-
V-2	O-5	1.717(2)	1.637(4)	-
V-2	O-6	1.635(4)	1.548(6)	-
V-2	O-7	1.717(2)	1.637(4)	-
V-3	O-4	1.717(2)	1.637(4)	-
V-3	O-3	1.717(2)	1.637(4)	-
V-3	O-2	1.635(4)	1.548(6)	-
V-3	O-1	1.809(1)	1.717(2)	-

431
432

This is a preprint, the final version is subject to change, of the American Mineralogist (MSA)
Cite as Authors (Year) Title. American Mineralogist, in press.
(DOI will not work until issue is live.) DOI: http://dx.doi.org/10.2138/am.2013.4335

433 **Table 2** Bond angles in the VO_5 pyramid in $K_2VV_2O_8$, $Rb_2VV_2O_8$, and $Ba_2VSi_2O_8$ (cf.

434 Fig. 2).

435

Atom 1	Atom 2	Atom 3	Angle [°]		
			$K_2VV_2O_8$	$Rb_2VV_2O_8$	$Ba_2VSi_2O_8$
O-7	O-8	O-9	90.0(1)	90.0(1)	90.0(3)
O-8	O-9	O-10	90.0(1)	90.0(1)	90.0(3)
O-9	O-10	O-7	90.0(1)	90.0(1)	90.0(3)
O-10	O-7	O-8	90.0(1)	90.0(1)	90.0(3)
O-11	V-1	O-7	106.73(6)	106.99(11)	107.91(37)
O-11	V-1	O-8	106.73(6)	106.99(11)	107.91(37)
O-11	V-1	O-9	106.73(6)	106.99(11)	107.91(37)
O-11	V-1	O-10	106.73(6)	106.99(11)	107.91(37)

436

437

438 **Table 3** Bond angles in the V_2O_7 group in $K_2VV_2O_8$ and $Rb_2VV_2O_8$ (cf. Fig. 2).

Atom 1	Atom 2	Atom 3	Angle [°]	
			$K_2VV_2O_8$	$Rb_2VV_2O_8$
O-1	O-2	O-4	60.72(8)	60.48(10)
O-2	O-4	O-1	58.56(6)	59.05(10)
O-4	O-1	O-2	60.72(8)	60.48(10)
O-1	O-2	O-3	59.67(7)	59.50(13)
O-2	O-3	O-1	60.66(7)	60.99(13)
O-3	O-1	O-2	59.57(7)	59.50(13)
O-2	O-3	O-4	61.56(6)	61.54(11)
O-3	O-4	O-2	58.39(5)	58.61(11)
O-4	O-2	O-3	60.05(6)	59.85(11)
O-1	O-3	O-4	61.56(6)	61.54(11)
O-3	O-4	O-1	58.39(5)	58.61(11)
O-4	O-1	O-3	60.05(6)	59.85(11)
O-4	O-5	O-7	60.72(8)	60.48(10)
O-5	O-7	O-4	60.72(8)	60.48(10)
O-7	O-4	O-5	58.56(6)	59.05(10)
O-4	O-5	O-6	60.05(6)	59.85(11)
O-5	O-6	O-4	61.56(6)	61.54(11)
O-6	O-4	O-5	58.39(5)	58.61(11)
O-5	O-6	O-7	60.66(7)	60.99(13)
O-6	O-7	O-5	59.67(7)	59.50(13)
O-7	O-5	O-6	59.67(7)	59.50(13)
O-3	O-6	O-7	61.56(6)	61.54(11)
O-6	O-7	O-3	58.39(5)	58.61(11)
O-7	O-3	O-6	60.05(6)	59.85(11)

This is a preprint, the final version is subject to change, of the American Mineralogist (MSA)
Cite as Authors (Year) Title. American Mineralogist, in press.
(DOI will not work until issue is live.) DOI: http://dx.doi.org/10.2138/am.2013.4335

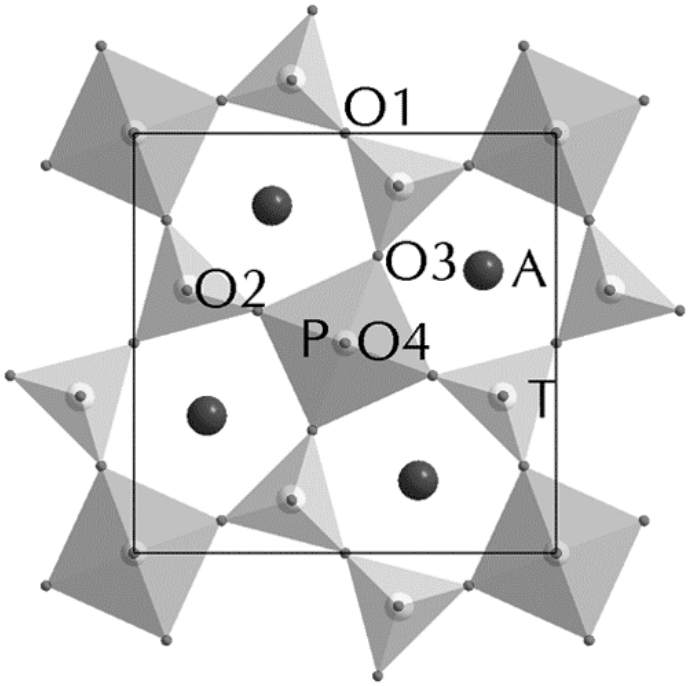

439

440

441

442 **Figure 1**

443

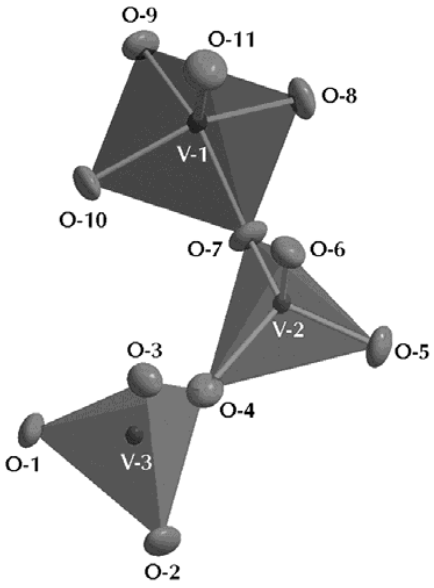

444

445

446 **Figure 2**

447

This is a preprint, the final version is subject to change, of the American Mineralogist (MSA)
Cite as Authors (Year) Title. American Mineralogist, in press.
(DOI will not work until issue is live.) DOI: http://dx.doi.org/10.2138/am.2013.4335

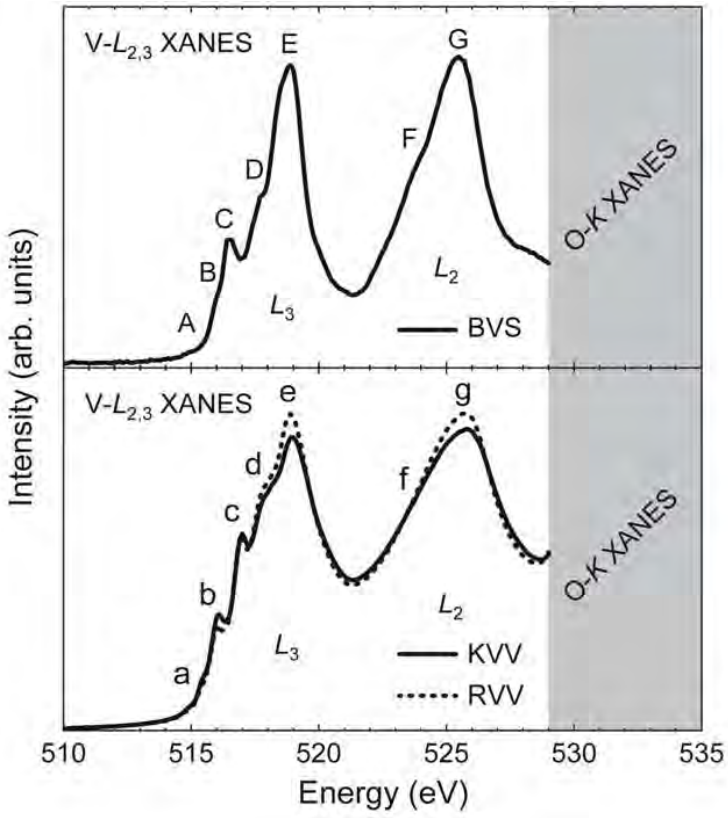

Figure 3

This is a preprint, the final version is subject to change, of the American Mineralogist (MSA)
Cite as Authors (Year) Title. American Mineralogist, in press.
(DOI will not work until issue is live.) DOI: http://dx.doi.org/10.2138/am.2013.4335

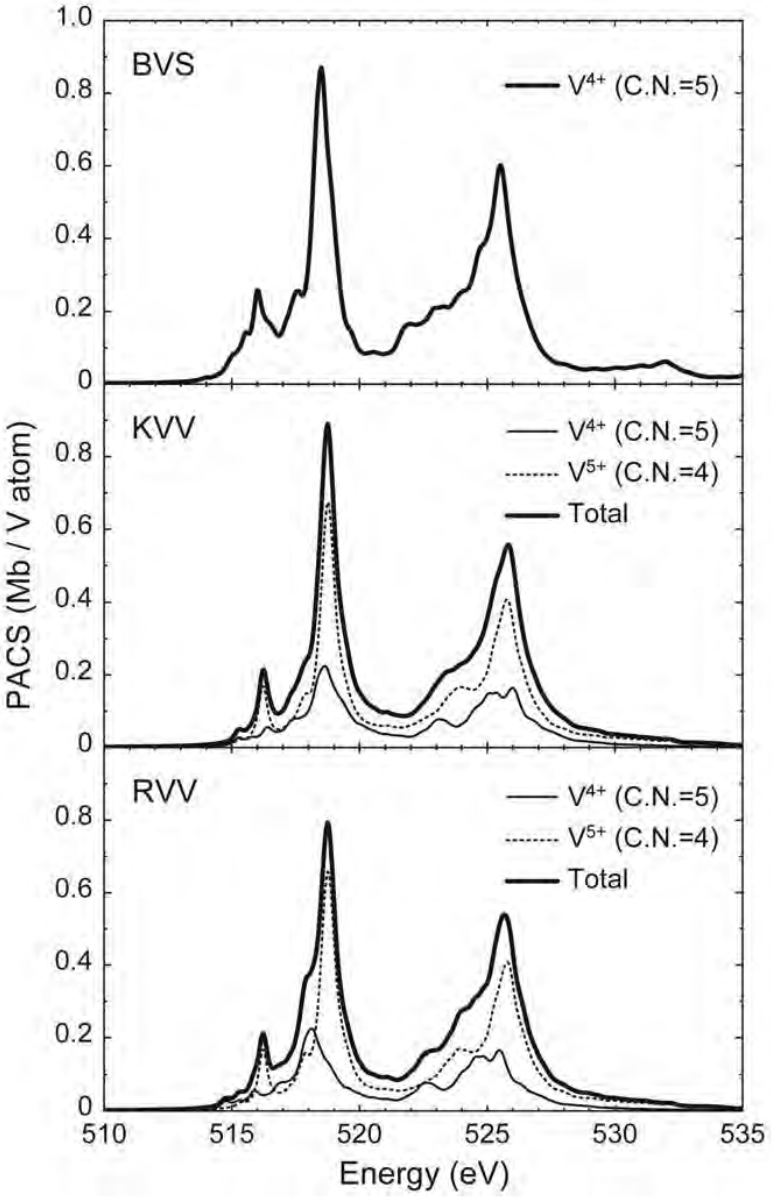

Figure 4

This is a preprint, the final version is subject to change, of the American Mineralogist (MSA)
Cite as Authors (Year) Title. American Mineralogist, in press.
(DOI will not work until issue is live.) DOI: http://dx.doi.org/10.2138/am.2013.4335

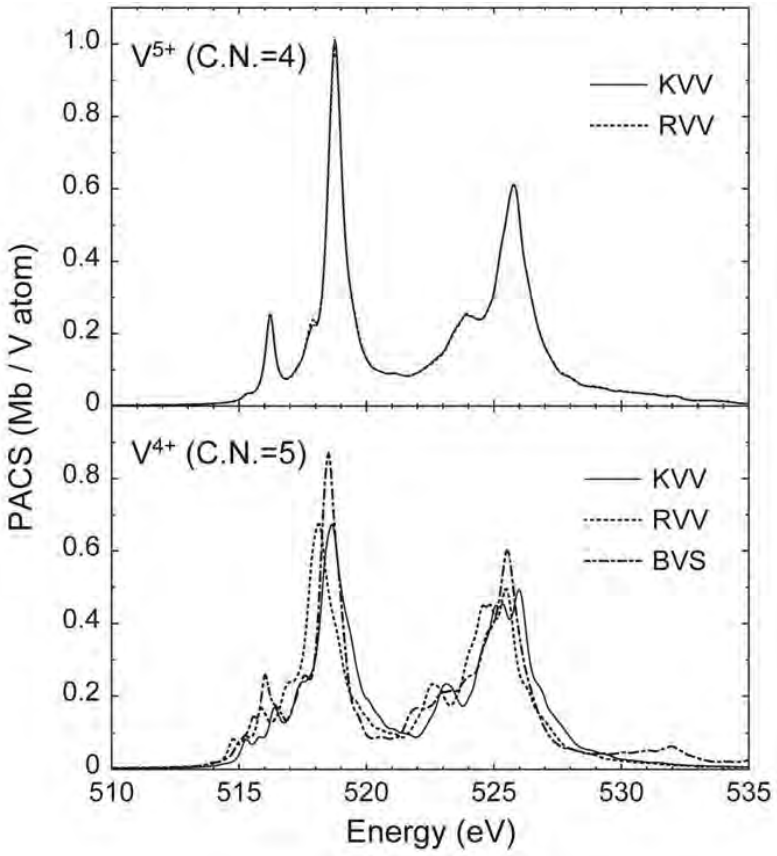

Figure 5